Carapace dissolution, growth decline and mechanoreceptor damages in Dungeness crab related to severity of ocean acidification gradients

Authors: Nina Bednaršek[1], Richard A. Feely[2], Marcus W. Beck[1], Simone R. Alin[2], Samantha A. Siedlecki[3], Piero Calosi[4], Emily L. Norton[5], Casey Saenger[5], Jasna Štrus[6], Dana Greeley[2], Nikolay P. Nezlin[1], John I. Spicer[7]

Affiliations:

[1]Southern California Coastal Water Research Project, Costa Mesa, CA, 92626 USA

[2]NOAA Pacific Marine Environmental Laboratory, 7600 Sand Point Way NE, Seattle, WA, 98115 USA

[3]Department of Marine Sciences, University of Connecticut, Groton, Connecticut 06340

[4]Département de Biologie, Chimie et Géographie, Université du Québec à Rimouski, 300 Allée des Ursulines, Rimouski, QC G5L 3A1, Canada

[5]Joint Institute for the Study of the Atmosphere and Ocean, University of Washington, Seattle, WA, 98195 USA

[6]Department of Biology, Biotechnical Faculty, University of Ljubljana, Ljubljana, Slovenia

[7] University of Plymouth, School of Biological and Marine Sciences, Plymouth PL4 8AA, UK

*__Corresponding author:__ Nina Bednaršek (ninab@sccwrp.org); (714) 755-3237

Running title: Dungeness crab sensitivity to acidification

Keywords: Dungeness crab, larval sensitivity, global climate change, ocean acidification variability, carapace minerology, elemental structure, carapace damage, mechanoreceptor loss, risk assessment.

Abstract:

Ocean acidification (OA) along the US West Coast is intensifying faster than observed in the global ocean. This is particularly true in nearshore regions (< 200 m) that experience a lower buffering capacity while at the same time providing important habitat for ecologically and economically significant species. While the literature on the effects of OA from laboratory experiments is voluminous, there is little understanding of present-day OA *in-situ* effects on marine life. Dungeness crab *(Metacarcinus magister)* is perennially one of the most valuable commercial and recreational fisheries. We focused on establishing OA-related vulnerability of larval crustacean based on mineralogical and elemental carapace to external and internal carapace dissolution. Using a combination of physical, chemical, biological, and modelling aspects, we identify the occurrence of external carapace dissolution related to the steepest Ω calcite gradients ($\Delta\Omega_{cal,60}$) in the water column. Dissolution features are observed across the carapace, legs, and around the calcified areas surrounding neuritic canals of mechanoreceptors. The carapace dissolution impact is greatest under 1-month long exposure as simulated by the use of model hindcast. Such dissolution has a potential to destabilize mechanoreceptors with important sensory and behavioral functions, a pathway of sensitivity to OA that has so far, to our knowledge, not been explored. Carapace dissolution is negatively related to crab growth, providing a basis for energetic trade-offs, while population dynamics are driven by the temperature and food availability. Using a retrospective prediction from a regression models, we estimate an 8.3% increase in external carapace dissolution over the last two decades and identified a set of affected OA-related sublethal pathways to inform future risk assessment studies of Dungeness crabs.

Introduction

Since the pre-industrial era, anthropogenic CO_2 uptake along the US West Coast have resulted in rapid intensification OA rate on a global scale (Chavez et al., 2017; Feely et al., 2016). This is because of the low regional buffering capacity, which contributes to low pH and carbonate mineral saturation states for both aragonite (Ω_{ara}) and calcite (Ω_{cal}) (Feely et al., 2018). These changes in carbonate chemistry have results in substantially reduced habitat suitability for marine calcifiers (Bednaršek et al., 2014; Somero et al., 2015). These findings are supported by the field and synthesis work along the North American Pacific demonstrating that calcifying invertebrates will be the ones most impacted by progressive OA (Bednaršek et al., 2017; Busch & McElhany, 2016). Apart from evidence of OA impacts on pteropods and other calcifiers caused by the low Ω_{ara} conditions in upwelling systems (Bednaršek et al., 2014, 2017) and around CO_2 vent seeps and sites (Manno et al., 2019; Tunnicliffe et al., 2009), there is limited understanding of present-day OA effects on marine life *in situ*. That is especially relevant for the crustaceans since they were considered less sensitive to OA parameters (like pCO_2 or pH) after studies demonstrated their capacity to abate initial hypercapnia and to buffer extracellular acid-base disturbances (Melzner et al., 2009; Pane & Barry, 2007) with limited or no change in aerobic metabolism (Paganini, Miller, & Stillman, 2014). However, restoring internal pH to sustain physiological and biogeochemical processes (Somero, 1986), typically requires an activation of energetically-expensive buffering of differential mechanisms (Cameron, 1985; Michaelidis, Ouzounis, Paleras, & Pörtner, 2005). Recent experimental findings have demonstrated increased sensitivity to OA-related stressors in crustaceans, especially in the early life stages that can be regarded as a potential bottleneck for the population level responses (Schiffer, Harms, Pörtner, Mark, & Storch, 2014; Small, Calosi, Boothroyd, Widdicombe, & Spicer, 2015). Regardless of the habitats different species inhabit, the

studies investigating OA effect on larval stages reported lower growth and decreased survival of blue crab (Giltz & Taylor, 2017), delayed metamorphosis in the stone crab (Gravinese et al., 2018), exoskeleton composition (Page, Worthington, Calosi, & Stillman, 2016) and metabolic rates in Tanner crabs (Long, Swiney, & Foy, 2016) and increased energetic costs in the porcelain crab (Carter et al., 2013).

With annual revenues up to $220 million (Hodgson et al., 2018; Pacific States Marine Fisheries Commission, 2019), the Dungeness crab (*Metacarcinus magister*) is one of most valuable and recreational fisheries in the US coastal waters. Terminal stage of pelagic Dungeness crab larvae (megalopae) can undergo long distance transport along the north Pacific coast of North America before settling in suitable benthic settlement site (Shanks, 1995; Sinclair, 1988). Given their diel vertical migration extends down to 60 m depth (Hobbs, Botsford, & Thomas, 1992), megalopae encounter low pH, Ω_{cal} conditions, as well as strong pH, Ω_{cal} gradients in coastal habitats; however, the duration and magnitude of their exposure to these conditions remains largely unknown despite the exposure history notably impacting organismal responses (*sensu* Bednaršek et al. (2017).

To identify potential OA vulnerability of this species in situ, their spatial distribution must be paired with an observations of their structural and mineralogical features, in situ exposure history, and knowledge of their physiological susceptibility. However, surprisingly little is known about the larval structural, crystalline, and mineralogical features that can predispose an individual to dissolution if the conditions in the external environment are conducive for it. In addition, for detecting environmental clues, decapod exoskeleton contains elongated hair-like structures called setae, which are important chemo- and mechanoreceptors involved in sensory and behavioral responses. While the lipoproteic epicuticle-covered carapace consists of two cuticular mineral

carbonate layers (Chen, Lin, McKittrick, & Meyers, 2008) (i.e., the outer exocuticle and the inner endocuticle) in the Dungeness crab adults such structure or its content is completely unknown for the larvae. At the individual level, pre-larval (zoeae) Dungeness crab show reduced survival and delayed development. This has been observed in multiple larval crab species (Giltz & Taylor, 2017; Gravinese, Enochs, Manzello, & van Woesik, 2018; Miller, Maher, Bohaboy, Friedman, & McElhany, 2016; Schiffer et al., 2014; Walther, Anger, & Pörtner, 2010) that could lead to changes in larval dispersal patterns and ultimately to larger population-level responses patterns.

To close the gap on *in situ* OA-related megalopae vulnerability, this interdisciplinary study integrates physical, geochemical, biological, and modelling components across the individual and population-level responses, using a comprehensive understanding of larval mineralogical and crystalline characteristics as a baseline to understand the effects of in situ exposure history on observed biological responses. First, we determined carapace mineralogical and elemental composition; second, we investigated structural and morphological features of megalopae exposed to large gradients related to the OA conditions along the North American West Coast; and third, to explore the effects on Dungeness megalopae we compared biological condition with chemical observations, in addition to using biogeochemical model hindcasts to determine how prolonged exposure history over the month prior to collection affected megaloape responses.

Materials and methods

Carbonate chemistry, sampling and analyses

For the purpose of this study, the NOAA West Coast Ocean Acidification (WCOA) cruise in May–June 2016 sampled conductivity, temperature, depth, and oxygen. CTD data were collected along

cross-shelf transects, accompanied by biological stations with vertical sections of temperature (T), salinity, nutrients, oxygen, chlorophyll-a (chl-a), dissolved inorganic carbon (DIC), total alkalinity (TA), spectrophotometric pH (measured at 25°C and corrected to *in situ* temperatures, and expressed on the total pH scale, subsequently expressed pH_T). pCO_2 and calcite saturation state (Ω_{cal}) were calculated using CO2SYS as described by Feely et al. (2016) and Bednaršek et al. (2012). Crabs were collected using Neuston and Bongo nets with a mesh size of 333 μm, which were deployed in an oblique manner at 13 stations during the night in the upper surface waters, an area that encompasses the nocturnal vertical habitat of larval Dungeness crabs of the upper 60 m (Hobbs et al., 1992; Morgan, 1985), with the following environmental parameters along the vertical habitat (Table S1). The duration of tows was 15–20 min. Megalopae were identified and then stored in 100% non-denatured ethanol, and also flash-frozen at -80 °C for later comparison of two different preservation methods.

Using SEM methods to detect and evaluate carapace dissolution

Megalopae carapaces were investigated using a combination of different methods: 1) scanning electron microscopy (SEM; Hitachi Phenom, USA) to determine potential structural changes on the exo- and endocuticle; 2) energy dispersive X-ray spectroscopy (EDXS at the University of Washington) for mineralogical composition; 3) elemental mapping; and X-ray diffraction (University of Washington and Max Planck Institute) for elemental content across mostly lipoproteic carapace (Figure S1, Fig. 1). The carapace epicuticle, which otherwise overlies the crystalline layer and makes dissolution observations impossible, was removed from each megalopa prior to analysis. This was accomplished using sodium hypochlorite, which efficiently removes the epicuticle but does not damage the crystalline layers underneath, even at high concentrations (Bednaršek et al., 2012). We tested different concentrations and duration of hypochlorite treatment

to ensure that we fully removed the epicuticle, without triggering dissolution of the calcite crystalline layers beneath it. For that, we tested 1, 3, and 6 % hypochlorite for 15 min, 30 min, 2, 4, and 6 hours exposure times, and compared these to an untreated control. On the samples with no hypochlorite treatment, the exoskeleton was completely covered by the epicuticle, and no investigation of dissolution was possible. The combination of 1 and 3 % sodium hypochlorite with 15, 30, and 120 min treatments only partially removed the epicuticle, with the epicuticle mostly still covering the upper crystalline layer, while 6% hypochlorite treatments for 4 and 6 h were equally effective in its removal, without inducing additional dissolution at the longer duration. Finally, we determined 6% hypochlorite for 3-4 h to be an efficient and effective treatment, similar to the treatment previously described for the removal of the periostracum in pteropods (Bednaršek et al., 2012). After soaking in sodium hypochlorite, samples were rinsed several times in Millipore water to remove any organic matter remaining on the surface of the exoskeleton. It is important to note that when examining the presence of setae within the neuritic canals, we did not use any treatment in order to avoid any methodological artifacts. The crystalline layers on the exo- and endocuticular surface of carapace, and external side of the pereopods were observed under SEM to quantify to quantify the extent and severity of dissolution. When examining the internal side of the cuticle, we avoided larger areas around the gills given their exposure to the external environment. We focused on three distinct features: ridging structures, dissolution around setae, and exposed calcite crystals (Figure S2, S3). To observe the internal carapace cuticle, the larvae's legs and soft tissue were gently removed from the rest of the body and washed in Millipore water to remove any remaining tissue or organics before treatment with sodium hypochlorite.

For estimating the growth across various OA gradients, we have measured carapace length (CL), total length from rostrum to telson (TL), length from rostrum to dorsal carapace spine (R-

DCS), and carapace width (CW), the last being latter the most common growth measure used by various US federal agencies along the US West Coast to regulate crab management catch efforts (Davis, Sylvia, Yochum, & Cusack, 2017). Using the methodology to characterize the megalopae stages by González-Gordillo et al. (2004), we determined that all megalopae were in the intermolt stage, except for those from Station 115, which were transitioning into the premolt stage. To avoid misinterpretation of dissolution patterns, we excluded the internal dissolution observations from that station.

Semi-quantitative dissolution assessment

Altogether, we analyzed 50 individuals from 10 environmental stations across OA-related gradients of varying strength. We used 3–5 individuals per station to determine dissolution extent on the external side of the exocuticle and pereopods, and an additional 2–3 individuals per station to analyze the internal side of endocuticle. Approximately 10–20 SEM images were produced per individual on the external and internal side, with the images being manually examined to detect any signs of dissolution. For crystal exposure characterization, the same categorization of dissolution conditions as previously described in pteropods was used (Bednaršek et al., 2012). We identified three major features of shell dissolution and developed a categorization scheme for all three features, showing them in their intact forms (Stage 0, Figure S2) and progressively altered forms (Stage 1 and 2; Figure S1; Table S2). These features differentiated damaged surfaces from the intact surfaces (Table S2). The surface of crab carapaces and pereopods under high *in situ* conditions had a smooth, sleek appearance (Figure S2; Stage 0). At greater magnification, individual calcite crystals were visible in these areas (Figure S2). Signs of dissolution tended to be more prevalent and more severe on the surface immediately surrounding setae pores. Consequently, areas around the setae were considered separately from the rest of the shell. From

these observations, a semi-quantitative scoring metric was developed based on previous work on pteropods and used to score the remainder of the samples. For each sample, the three separate features (presence and depth of ridge structures, exposure of individual calcite crystals, and the prevalence of dissolution features around setae pores) were each assigned a score. The features were scored on a scale of 0 to 1 based on the severity of dissolution: intact shell with no dissolution received a score of 0; moderate dissolution received a score of 0.5; and substantial dissolution of all examined features was scored 1 (Figures S1–S3). Since the crab carapace and pereopod cuticle differ in their chemical composition, these three areas were assigned separate scores. Because of the surface analyses required separately for the external and internal dissolution, both types of analyses could not be conducted on the same individual. All three features displayed similar trends, so the scores were averaged to unitless 'relative dissolution', describing internal and external dissolution. Observation of setae presence/absence was included in the carapace observation under SEM on intact specimen before any preparation treatments were conducted to eliminate the possibility of preparation steps affecting setae presence or outrooting them from the carapace.

Mineralogical analyses

The mineralogy of selected megalopae was characterized using X-ray diffraction (D8 Discover 2D; University of Washington, Seattle). Prior to analysis, carapaces from five megalopae at each site were coarsely crushed and treated for 10 min using a dilute (3%) sodium hypochlorite solution to minimize interference from organic matter but without compromising mineralized structures. Samples were dried completely and then ground to a fine homogenous powder representing the aggregate of the five individuals from each location. Resulting diffractograms were compared to a catalog of mineral-specific patterns to constrain the primary mineralogy of each sample.

Elemental analyses

We used energy-dispersive X-ray spectroscopy (EDXS) to estimate elemental composition of the carapace and leg cross-sections (N = 7) from samples across different natural OA gradients. For elemental analyses, we have not removed the epicuticle from the samples. These gradients analyses were conducted at Max Planck Institute for Marine Microbiology in Bremen, Germany. Prior to analyses, we dehydrated samples using 100 % ethanol and dried them in a critical point dryer. We prepared the sections by fracturing different carapace regions which was followed by the EDXS investigations (Figure 1).

Statistical analyses

Biological measurements from Dungeness megalopae collected at 10 stations along the North American Pacific Coast (Figure 2) were paired with synoptic environmental data from CTD profiles. Environmental data were summarized as depth-integrated averages from the surface to the maximum depth of each CTD profile to characterize the exposure conditions in the upper water column. In addition, $\Delta\ \Omega_{cal,60}$ was estimated as the difference from the observed measurement at each depth bin with that of the surface. This measurement characterized the relative Ω_{cal} gradients with increasing depth and accounted for differences in the relative magnitudes of Ω_{cal} between stations. Chlorophyll-a observations were highly skewed and so were log-transformed prior to analysis.

Biological responses included dissolution, length extension, and abundance with various environmental gradients to identify significant associations using generalized linear models. For comparison of the biological data to environmental gradients, each depth bin for the depth-integrated values was evaluated to identify at which depth associations between biological response and selected environmental variables were strongest. In addition, carapace dissolution was compared to length and presented data to characterize potential links of physiological

parameters (carapace dissolution) with growth (length) and population-level effects (abundance). Comparisons of biological measures to each other were also accomplished with generalized linear models.

Gaussian distributions were assumed for all response variable models, excluding presence/absence, which was modeled using a binomial logistic response curve. Models and individual parameters were considered significant at $\alpha = 0.05$. All models had N = 10 except presence/absence models with N = 24, which included additional stations where tows were conducted but no crabs were found. Finally, all variables were evaluated together to identify pairwise associations using Pearson correlation analysis and redundancy analysis (RDA) to characterize how the biological response measures were jointly explained by the environmental variables. For the latter analysis, all input data were standardized to range from 0 to 1 to account for differences in scale between variables. The *vegan* package for the R statistical programming language was used for standardization and RDA (Oksanen et al., 2019; R Core Team, 2019).

For selected predictors, additional models were developed to evaluate the additive effects of two predictors on dissolution. Backward model selection was used to identify the most parsimonious model by sequentially dropping individual predictors and comparing Akaike Information Criterion values (AIC) (Akaike, 1973; Fox & Weisberg, 2011). This allowed us to determine if there was any additional power in combining predictors to explain dissolution, or consequently, if dissolution could be sufficiently explained using only one predictor. For example, the ability of both Ω_{cal} and chlorophyll to explain dissolution were evaluated to better understand the relative effects of both.

J-SCOPE model outputs of the larval exposure history prior to sampling

The Joint Institute for the Study of the Atmosphere and Ocean (JISAO)'s Seasonal Coastal Ocean Prediction of the Ecosystem (J-SCOPE, http://www.nanoos.org/products/j-scope/) features dynamical downscaling of regional ocean conditions in Washington and Oregon waters (Siedlecki et al., 2016). Model performance and predictability examined for sea surface temperature (SST), bottom temperature, bottom O_2, pH, and Ω_{ara} through model hindcast, reforecast, and forecast comparisons with observations, showing significant measurable skill on seasonal timescales (Kaplan, Williams, Bond, Hermann, & Siedlecki, 2016; Siedlecki et al., 2016)**.** Megalopae exposure histories were simulated by releasing 100 representative particles, with vertical migration behavior over 60 m inserted into the predicted circulation field at each of the *in situ* sampling locations and times, and then tracking them backward in time for 30 d. The vertical migration behavior was simulated using the LTRANSv2b larval transport model (North et al., 2008, 2011; Schlag & North, 2012) that has recently been implemented in the J-SCOPE system and adapted for megalopae.

Results

Elemental and crystalline characterization of the carapace

The compilation of our results demonstrate that the carapace is highly mineralized and precipitated into a chitin-proteinaceous matrix. XRD identify calcite as a primary polymorph in the carapace. The mineralized exoskeleton of the megalopae intermolt stages consists of the thinner exocuticle on the surface that is less than 2–3 µm thick, and the thicker and more compact endocuticle underneath (Figure 1) of approximately 6–7 µm, with the combined thickness up to 10 µm. The carapace surface is extensively covered with setae that are rooted in the calcified neuritic canals each with an average of about 5 µm surface opening (Figures S2 and S3). EDXS investigations

characterized detailed elemental structure with average Ca^{2+} content of 28 % in the carapace and pereopods, with much higher Ca^{2+} found within in the mid layer and the endocuticle (higher than 50%) compared to less than 20% found in the exocuticle (Figure 1). The carapace endocuticle contains also a high concentration of Mg^{2+} with some areas of the carapace exceeding 5% content, categorizing it as a more soluble high-Mg calcite. In addition, the internal side contain high concentrations of phosphorus (up to 6%) and strontium (up to 2%) on the inner endocuticle (Figure 1). The percentage of different elements is similar in the carapace as well as in the pereopods, however with much less variation in all elements between the carapace and pereopods (Figure S1). This elemental composition indicates that other crystalline forms of carbonate could be precipitated into a chitin-proteinaceous matrix, such as an amorphous crystalline layer, but the methods we have used are not capable of the detection. The strong presence of autofluorescence prevented more precise detection of any other crystalline forms, despite extensive use of Raman spectroscopy for this purpose. Nevertheless, such elemental structure resembles a layer of amorphous calcium carbonate (ACC) with Mg^{2+}, phosphate and carbonate-rich phase, or ACC with magnesian calcite, as previously demonstrated in the edible crabs *Cancer pagurus* (Fabritius et al., 2012).

Megalopae habitat characterization with strong vertical and spatial Ω_{cal} gradients

Crab megalopae were found in both outer-shelf, slope, as well as nearshore (<200 m depth) habitats, with distinctly different environmental gradients in the upper water column. Due to the upwelling of deeper, colder, CO_2-rich waters with relatively low Ω_{cal} in the nearshore steep vertical gradients in pH and Ω_{cal} values were observed in the upper 60 m of the water column, compared to the offshore region over the same depth interval (Figure 2). Consequently, models comparing

biological response measures with environmental conditions had the strongest associations using the 60 m vertical depth integrated value (e.g., external dissolution on body parts vs. $\Delta\Omega_{cal}$ had the highest $R^2 = 0.821$ at 60 m). Hereafter, all environmental data are reported using the 60 m depth integrated averaged values. Coastal conditions at the same locations at 60 m recorded near-saturation Ω_{cal} values down to 1.4, pH down to 7.48, pCO_2 up to 910 uatm, and at 60 m depth (Table S1; Figure 2). Pronounced steep OA-related vertical habitats were observed in the upper 60 m of the water column, here represented as the difference between the surface and 60 m depth ($\Delta\Omega_{cal,60}$ or ΔpH_{60}), which is within the lower range of megalopae diel vertical migration habitat. There were no observations of $\Omega_{cal} < 1$ or hypoxia, with similar oxygen ranges observed in the onshore and offshore regions, while average temperature that was by about 1.3° C warmer offshore. Food availability was an order of magnitude higher in the onshore regions compared to offshore, with the highest chl-a values recorded at 25 $\mu g\ L^{-1}$ (Figure 2).

Multiple environmental parameters co-varied (Figure 3) as observed in the RDA plot at 60 m depth (Figure 3). The first two axes of the RDA explained approximately 90% of the variation among the biological and environmental parameters. The first RDA axis was characterized by a gradient in $\Delta\Omega_{cal,60}$ and external dissolution, with both having negative loadings along the RDA1 axis. Carapace width was negatively correlated with $\Delta\Omega_{cal,60}$, whereas external dissolution was positively correlated, suggesting that larger individuals had less dissolution and were associated with lower gradients in $\Delta\ \Omega_{cal,60}$. While OA parameters (pCO_2, pH) were all correlated as indicated by alignment with the second RDA axis, the collinearity with temperature was not significant. We found less collinearity among the environmental parameters related to the 60 m gradients, such as $\Delta\Omega_{cal,60}$, $\Delta O_{2,60,}$ and ΔT_{60}. However, focusing on the mechanistic drivers rather than on all the parameters that are not explicitly involved in the external dissolution processes, we have only

examined $\Delta\Omega_{cal,60}$ in how it relates to external dissolution. Similarly, internal dissolution was negatively correlated with pCO_2 along the second axis with slightly higher loading along the RDA1, and also slightly negatively related with increased temperature. The implications of this association and how they related to model output (Figure 7) will be explained below.

Megalopae carapace dissolution and growth as responses to variable OA parameters across vertical scales

Dissolution assessment on the external surface of the exocuticle and internal surface of the endocuticle of the megalopa's exoskeleton and legs, was conducted only after confirming that sample preservation did not impact dissolution patterns, i.e. samples preserved in ethanol vs. flash frozen did not exhibit any significant difference in their dissolution features. Using a novel categorization scheme to semi-quantify dissolution features, including ridging structures, dissolved areas around neuritic canals, and exposed calcite crystals (Figures 4, S1 and S2; Table S2), the individuals demonstrated various extents of that these features present on the external side of the carapace and the legs (Figure S2 and S3). On the carapace, the front and outer surfaces were the most affected (Figures 4 and S3). On the pereopods, the thoracic segments and chelae had the most severe dissolution, while the distant parts were less affected (Figure S3).

On all of the examined individuals with external dissolution, we also found evidence for internal endocuticle dissolution, which was, on average, approximately half that observed on the external exocuticle surface. Average dissolution on the exocuticle showed the strongest linear dependence with $\Delta\Omega_{cal,60}$ (Figure 5; $R^2 = 0.866$, $p < 0.001$), while the internal dissolution showed the most robust evidence, though not statistically significant, of correlation with pCO_2 values (Figure 5; $R^2 = 0.406$, $p = 0.065$) and negative marginal significance with temperature ($R^2 = 0.435$,

343 p = 0.053). The internal dissolution rapidly intensified beyond pCO_2 >500 uatm (Figure 5b), with
344 this being a robust threshold value. There was no significant correlation between internal and
345 external dissolution (Figure 5; p = 0.18), suggesting decoupling of the two processes.

346 At sites with a small $\Delta\Omega_{cal,60}$, the external surface of the carapace was characterized by
347 predominantly smooth surfaces, the absence of dissolution, and the presence of setae (Figures 7
348 and S2). Ridging features were present on all examined carapaces but significantly increased at
349 the stations with the greatest $\Delta\Omega_{cal,60}$ difference (Figures 4 and 5). This presence of ridging features
350 co-occurred with the increased occurrence of crystal exposure, ranging from increased porosity
351 (Stage 1) to exposed crystals (Stage 2) at the sites with lower $\Delta\Omega_{cal,60}$ difference, and deeper-
352 protruding dissolution at the sites with greater $\Delta\Omega_{cal,60}$ difference (Stage 2). Using image analysis,
353 the depth of ridging structures was estimated at approximately 2 µm, around 25% of the cuticle
354 thickness. Given the exocuticle thickness of 2–3µm, the dissolution extendede into the endocuticle
355 (Figure S4). The extent of dissolution on pereopods was comparable with the external dissolution,
356 especially at the higher dissolution values (Figure S5; R^2 = 0.65; p = 0.0047, slope = 0.901),
357 indicating that both features were reliable metrics for dissolution assessment.

358 There was a distinct pattern of severe dissolution specifically developed around the
359 calcified neuritic canals (Figure 6). In megalopae collected at inshore stations (< 200 m bottom
360 depth), the carapace surface around the neuritic canals was markedly dissolved (Stage 2), and
361 mechanoreceptors were often absent. Dissolution around the neuritic canals appeared to alter the
362 morphology of the setae (Figure 6). Setae edges were partially collapsed where the
363 mechanoreceptors are usually anchored and initial ridging features around the canals degenerated
364 into severely dissolved surfaces at the more intense $\Delta\Omega_{cal,60}$ values (Figure 6). On the megalopae
365 from offshore stations with a smaller $\Delta\Omega_{cal,60}$ the mechanoreceptors were present with no damage

366 around the neuritic canals and less severe dissolution. Within the region of altered setae,
367 dissolution up to 2–3 µm around the setae (Figure S4) was accompanied by significant canal
368 deformation. This deformation appears to destabilize the attachment of the setae anchor, resulting
369 in the setae 'outrooting'. In some of the calcified neuritic canals, we noted the absence of setae but
370 have not yet quantified the frequency of this occurrence.

371 To examine whether external or internal dissolution affects organismal or even potentially
372 population-level metrics, dissolution measures were compared to megalopae growth and
373 abundance. We detected a significant negative correlation between external dissolution and
374 growth, as indicated by reduced individual carapace width (CW; $F = 18.61$, $R^2 = 0.823$, $p = 0.013$
375 for the regression of CW against external dissolution on body parts; $F = 5.3$, $R^2 = 0.57$, $p = 0.08$
376 for the regression of CW against all external dissolution; Figure 5), which is particularly strong in
377 the coastal stations. This demonstrates that external OA-related exposure can indirectly affect
378 larval growth. Growth (width) as indicated by carapace width was strongly oriented along the first
379 RDA axis (Figure 3), while being orthogonal to internal dissolution and directly opposed to
380 external dissolution. The latter aligns with previous findings that internal dissolution is uncoupled
381 from growth (linear model $p > 0.05$), whereas external dissolution is significantly associated with
382 carapace width (RDA plot). Other growth-related parameters (CL, R-DCS, TL) were not affected
383 by OA parameters, demonstrating that only specific growth parameters, i.e., width, but not length,
384 are affected at more severe $\Delta\Omega_{cal,60}$ gradients.

385 On the higher, population-level response, only chl-a was found to be a significant driver.
386 Abundance was positively correlated with chl-a at 60 m depth for both onshore and offshore
387 habitats ($R^2 = 0.327$; $p = 0.008$). None of the other environmental parameters had a significant
388 impact. However, in shallow coastal habitats with depth <30 m, temperature was negatively related

to larval abundance (for temperature at 10 m, R^2 = 0.241; p = 0.02; F = 6.56), although chl-a remained the dominant driver. In addition, neither carapace dissolution nor growth was related to larval abundance, suggesting decoupling of individual- and population-level effects of environmental conditions on larval Dungeness during the present day.

Megalopae exposure history to coastal OA gradients during the month prior to sampling

Particle back-tracking results with simulated vertical migration between the ocean surface and 60 m depth over a 30-d period from the J-SCOPE simulations showed that megalopae that were released in coastal habitats (<200 m), remained in coastal habitat for nearly a month of simulation regardless of their position in the domain (Figure 7). This retention results in extended exposure to steeper OA coastal gradients (Figure 2), and consequently, more intense dissolution (Figure 5).

Discussion

To our knowledge this is the first time that OA-related dissolution of calcite structures *in situ* has been demonstrated for crustaceans. Our results indicate that it is the exposure to both parameters, $\Delta\Omega_{cal,60}$ (i.e. the difference in calcite saturation depth between the surface and 60 m depth) and pCO_2, set up by as well as prolonged (over 1 month) retention in the coastal waters that characterizes the suite of *in situ* parameters determining the larval crab vulnerability. This primarily demonstrates that it is not just the mean state OA conditions, but also the variability over the depth of the water column that can induce negative biological responses. Using a retrospective prediction from a regression models (Figure 5a), we estimate an 8.3% increase in the extent of external carapace dissolution over the last two decades. This post-hoc estimate was based on a ΔpH changes of 0.02 unit per decade (Carter et al., 2018) and comparing average current

411 dissolution with that predicted from our regression model based on the *in situ* observations (Figure
412 5a) by using the estimated pH conditions two decades prior. This is a reasonable estimate since
413 $\Delta\Omega_{cal,60}$ is highly correlated with $\Delta\Omega_{pH,60}$ ($F = 204.3$, $R^2 = 0.96$, $p < 0.001$, Figure S6).

414 What makes this OA-dependent dissolution of megalopae particularly relevant is that the
415 crab samples originated in the supersaturated conditions with respect to calcite (the lowest Ω_{calc}
416 =1.41). Since the dissolution reported in other calcifiers has been demonstrated above Ω_{ara} of 1.4–
417 1.5 (Bednaršek & Ohman, 2015; Bednaršek, Johnson, & Feely, 2016), we conclude that external
418 crab dissolution is initiated at higher $\Delta\Omega_{cal,60}$ than predicted based on thermodynamic principles
419 alone. Furthermore, using exposure metrics based on the biogeochemical model output
420 demonstrates that 1-month long exposure in coastal habitats with large $\Delta\Omega_{cal,60}$ values can result
421 in significantly more dissolution than predicted based on snap-shot observational data. In
422 comparison with the chemical observations, particle tracking model output indicates prolonged
423 severity of exposure to the coastal low OA conditions, allowing for more extensive carapace
424 dissolution and reduced growth in those habitats. It is worth noting that dissolution could be
425 viewed as a physiological strategy to compensate against unfavorable external conditions.
426 Dissolution of the outer calcite layer could increase the release of the bicarbonate and hydroxyl
427 ions, raising pH, and providing a rapid alkalinization of the superficial layer (Kunkel, Nagel, &
428 Jercinovic, 2012). This alkaline layer could then provide an additional local protection from
429 exposure to a large $\Delta\Omega_{cal,60}$ conditions by blocking protons from continuously invading the internal
430 fluid However, as the larvae live in highly dynamic environments, such a layer would be
431 continuously disrupted, explaining the high extent of external dissolution.

432 ***Dissolution as a mechanism to offset OA-related extracellular acid-base disturbance?***

Species with a developed capacity for ion exchange to maintain extracellular acid-base balance, are able to compensate for the effects of exposure to high pCO_2 waters and restore extracellular pH values optimal for physiological and biogeochemical processes (Somero, 1986). They do so via energetically expensive buffering of intra- and extracellular compartments achieved through various mechanisms, including active H^+ ion pumping to the external environment, buffering by seawater-derived bicarbonate sources (Truchot, 1979), increased respiratory activity to reduce CO_2 loading of the extracellular fluid and non-bicarbonate buffering (Cameron, 1985; Hans, Fehsenfeld, Treberg, & Weihrauch, 2014; Michaelidis et al., 2005). However, the downside to the well-established extracellular acid-base control is an energetically demanding process (Hans et al., 2014; Michaelidis et al., 2005; Pane & Barry, 2007; Trigg et al., 2019). Therefore, we hypothesize that the internal carapace dissolution we observed in our study could be a part of a passive ability to buffer reductions in extracellular pH. Mobilization of bicarbonate ions into extracellular spaces to buffer low pH through internal dissolution of the carbonate exoskeleton is a feature found in a variety of marine invertebrates including bivalves, echinoderms, and crustaceans (Cameron, 1985; Henry, Kormanik, Smatresk, & Cameron, 1981; Lindinger, Lauren, & Mcdonald, 1984; Spicer & Taylor, 1987; Spicer, Raffo, & Widdicombe, 2007). The narrow neuritic canals around the mechanoreceptors allow communication through secretion across the internal-external cuticle layers (Kunkel et al., 2012). While we currently have no information on the acid-base balance within these larval crabs under prolonged exposure to steep pCO_2 gradients because no controlled experiments have been conducted, we propose future studies to examine if internal dissolution could provide some level of bicarbonate ions for buffering at comparatively low cost. However, given that bicarbonate ions might also easily penetrate through the gills, thus potentially not being

455 limited parameter, our assumption of 'passive acid-base buffering by larval carapace dissolution',
456 urgently requires thorough testing.

457 Alternative hypothesis for explaining internal dissolution might be based on the severity of
458 external dissolution extending much deeper (Figure S4) to initiate the endocuticle dissolution.
459 Once the dissolution of the external carapace dissolution is initiated, the mineralogical-elemental
460 structure of the mid- and endocuticle can allow for more rapid progression. The presence of high-
461 Mg^{2+} content in the endocuticle can cause more rapid dissolution (Andersson, Mackenzie, & Bates,
462 2008), while comparatively lower Ca^{2+} content on the outward side presumably results in a weaker
463 carapace (Chen et al., 2008). Furthermore, while the internal solubility extent may be compensated
464 by phosphorus, it can increase hardness, thereby preventing propagation of fractures, and Sr^{2+}
465 because it can replace Ca^{2+} in the mineralization process (Dodd, 1964). In contrast, the observation
466 of lower dissolution on the internal surface compared to the exterior could be due to a difference
467 in biomineral composition. For instance, intermixing calcite in the endocuticle with organic
468 polymers would create a durable, protective covering, which may prevent the more soluble high-
469 Mg calcite in the endocuticle from dissolving (Chen et al., 2008). However, we have not found the
470 evidence of dissolution reaching throughout on the internal side of the endocuticle, and thus, we
471 propose an acid-base balance strategy to be more feasible explanation for the internal dissolution.

472

473 ***Potential detrimental effect associated with carapace dissolution***

474 One of the most important findings of this study is the correlation between carapace dissolution
475 and the reduction in larval growth. This could, overtime, potentially impact population dynamics.
476 We suggest that the dissolution-growth linkage could be explained by two different hypotheses:
477 first, pronounced dissolution under severe $\Delta\Omega_{cal,60}$ gradients results in dissolution rate outpacing

calcification rate. In this mismatch of rates of two different processes, calcification rate cannot fully compensate for dissolution and results in overall slower growth rates (‘*the mismatch’* growth hypothesis). Alternatively, there could be an energetic implication behind the dissolution-induced growth slowdown. In this form of the hypothesis, an organism expends additional energy to increase calcification to counteract dissolution, thus resulting in an energetic trade-off that compromises growth (the ‘*trade-off’* growth hypothesis).

Furthermore, for early Dungeness crab life stages in the near-future, the prediction of more frequent and prolonged exposures to more severe $\Delta\Omega_{cal,60}$ gradients (Turi, Lachkar, Gruber, & Münnich, 2016) could have potentially deleterious consequences in terms of behavioral and sensory impairments and pereopod function. First, dissolution-affected thinner structures may become too weak to retain their integrity, particularly under more severe conditions and continuous water flow, resulting in ridged, puffed surfaces. Morphological changes may in turn negatively impact larval survival by altering swimming behaviors and competence, including the ability to regulate buoyancy, maintain vertical position, and avoid predators (Morgan, 1989; Sulkin, 1984). Similar morphological structures as those observed in our study were noted in the larval form of the European lobster (Agnalt, Grefsrud, Farestveit, Larsen, & Keulder, 2013), which under prolonged exposure to OA conditions led to irreparable carapace deformities, and these could lead to an increase in molt-related mortalities (Small, Calosi, Boothroyd, Widdicombe, & Spicer, 2016). Second, dissolution on both sides of carapaces and pereopods will inevitably limit the effectiveness of the shell in providing support for muscles contraction and defense from predators, aiding homeostatic functions, and enabling feeding functions. Third, calcified neuritic canals appear to be one of the dissolution hotspots compromising setae function. Compared with undamaged setae at undissolved surfaces (Figures 7 and S2), dissolved areas may not provide

sufficient structural integrity for the setae (Figure 6), potentially impairing their functionality. Given the role of setae as mechanoreceptors directly involved in supporting crustacean sensory and behavior processes, we hypothesize that the absence or damage of setae within their neuritic canals may in part provide a mechanistic understanding for potential aberrant behavioral patterns found across various crustacean species under low OA conditions, such as slower movement, less tactile recognition, and prolonged searching time, as well as impaired swimming (Alenius & Munguia, 2012; Dissanayake & Ishimatsu, 2011) and behavioral choice (de la Haye, Spicer, Widdicombe, & Briffa, 2011). These changes can result in impaired competitiveness and altered predator-prey relationships for crabs (de la Haye, Spicer, Widdicombe, & Briffa, 2012; Dodd, Grabowski, Piehler, Westfield, & Ries 2015; Landes & Zimmer, 2012; Wang, Hu, Wu, Storch, & Pörtner, 2018). Fourth, it is currently unknown whether external dissolution in megalopae could carry over into later life stages, including the reproductively active adult stage, and what the potential consequences may be for the population dynamics. However, if the decreased growth and lower calcification could result in poor mineralization through the intermolt period that would be especially devastating for larval crabs because of potentially smaller sizes at maturity, as well as increased vulnerability to predation during their most sensitive molting stage.

While OA parameters largely affect observed biominerological and organismal responses, population-level responses (i.e. abundances) are driven by food availability, with a lesser role for temperature in the near-shore conditions. Although biological responses at different levels of biological organization appear to be decoupled and responded to different drivers across temporal and spatial scales that need to be taken into account to improve biological forecasts and predictions. The only driver that seem to resonate across individual and population level, at least marginally, is the temperature, which might have an opposite effect on both levels. While warmer temperature

524 negatively affects abundances, it also reduces internal dissolution, although the latter is only a
525 marginally significant.

526 To more accurately predict large-scale vulnerability, it is important to consider population
527 connectivity, related to essential population vital rates and affected by dispersal (Lowe &
528 Allendorf, 2010). This can be partitioned into genetic connectivity and demographic connectivity,
529 with our model outputs demonstrating onshore-offshore connectivity along the shelf-coastal and
530 in the northern-southern directions. This implies prolonged exposure to compressed suitable
531 habitats to low $\Delta\Omega_{cal,60}$ in the nearshore areas that can exacerbate negative biological effects but
532 some of them could be counteracted by higher food availability. With respect to genetic
533 connectivity, the status of Dungeness crab as a high gene-flow species with low genetic
534 differentiation along the US West Coast and the lack of significant adaptation patterns (Jackson &
535 O'Malley, 2017; Jackson, Roegner, & O'Malley, 2018; O'Malley et al., 2017) implies that the
536 genetic pool that might allow for adaptation under future climate scenario will be limited. This
537 points toward the need for more comprehensive population vulnerability assessment that can link
538 OA vulnerability with the population genetics.

539 ***Next steps***

540 Like dissolution in pteropods, crab larval dissolution is clear evidence that marine invertebrates
541 are damaged by extended exposure to strong present-day OA-related gradients in their natural
542 environment. The novel aspect of OA impacts are damaged mechanoreceptors where the level of
543 impaired sensory functions needs to be explored further. Namely, if the sensory functions are
544 impaired, the transitioning from the larval to juvenile stage in their core coastal habitat with
545 predicted intensification of ΔpH and $\Delta\Omega_{cal,60}$ (Gruber et al., 2012; Turi et al., 2016) might be
546 compromised. Multiple pathways of larval vulnerability should be studied in the context of carry-

over effects to the next juvenile benthic stage to explore whether crustacean molting can offset some of the detrimental effects. Such findings should be integrated into a population demographic and exposure history model that could eventually lead to improved management of Dungeness crab stocks (Fernandes et al., 2017; Lam, Cheung, Reygondeau, & Sumaila, 2016).

Acknowledgements: We thank Carry Weekes and Anna McLasky for collecting the larval individuals, Jennifer Fisher for providing guidance to Weekes; Sten Littmann from Max Planck Institute in Bremen, Germany for elemental analyses. We are grateful to Polona Mrak and Miloš Vittori for analyses of the crab molting stages. We thank NOAA's Ocean Acidification Program for initial funding and NOAA Pacific Marine Environmental Laboratory (PMEL) for supporting NB, RAF, and SAS. We are grateful to Sandra Bigley for her editorial help with the manuscript. This is PMEL contribution number 4906.

Competing financial interests: There were no competing financial interests.

References

Agnalt, A.-L., Grefsrud, E. S., Farestveit, M., Larsen, M., Keulder, F. (2013). Deformities in larvae and juvenile European lobster (*Homarus gammarus*) exposed to lower pH at two different temperatures. *Biogeosciences, 10,* 7883–7895.

Akaike, H. (1973). Information theory and an extension of the maximum likelihood principle. In: B. N. Petrov & F. Csaki (Eds.) Second International Symposium on Information Theory (pp. 267–281). Budapest, Hungary: Akademiai Kiado.

Alenius, B., Munguia, P. (2012). Effects of pH variability on the intertidal isopod, *Paradella dianae*. *Marine and Freshwater Behaviour and Physiology, 45*, 245–259.

Andersson, A. J., Mackenzie, F. T., Bates, N. R. (2008). Life on the margin: Implications of ocean acidification on Mg-calcite, high latitude and cold-water marine calcifiers. *Marine Ecology Progress Series, 373*, 265–273.

Bednaršek, N., Feely, R. A., Reum, J. C. P., Peterson, B., Menkel, J., Alin, S. R., Hales, B. (2014). *Limacina helicina* shell dissolution as an indicator of declining habitat suitability owing to ocean acidification in the California Current Ecosystem. *Proceedings of the Royal Society B: Biological Sciences, 281*, 20140123.

Bednaršek, N., Feely, R. A., Tolimieri, N., Hermann, A. J., Siedlecki, S. A., Waldbusser, G. G., McElhany, P., Alin, S. R., Klinger, T., Moore-Maley, B., Pörtner, H. O. (2017). Exposure history determines pteropod vulnerability to ocean acidification along the US West Coast. *Scientific Reports, 7*, 4526.

Bednaršek, N., Johnson, J., Feely, R. A. (2016). Comment on Peck et al: Vulnerability of pteropod (*Limacina helicina*) to ocean acidification: Shell dissolution occurs despite an intact organic layer. *Deep-Sea Research Part II: Topical Studies in Oceanography, 127*, 53–56.

Bednaršek, N., Ohman, M. D. (2015). Changes in pteropod distributions and shell dissolution across a frontal system in the California Current System. *Marine Ecology Progress Series, 523*, 93–103.

Bednaršek, N., Tarling, G. A., Bakker, D. C., Fielding, S. , Cohen, A. , Kuzirian, A. , McCorkle, D. , Lézé, B., Montagna, R. (2012). Description and quantification of pteropod shell

dissolution: A sensitive bioindicator of ocean acidification. *Global Change Biology*, *18*, 2378–2388.

Busch, D. S., McElhany, P. (2016). Estimates of the direct effect of seawater pH on the survival rate of species groups in the California Current Ecosystem. *PLoS One*, *11*, e0160669.

Cameron, J. N. (1985). Compensation of hypercapnic acidosis in the aquatic blue crab, *Callinectes sapidus*: the predominance of external sea water over carapace carbonate as the proton sink. *Journal of Experimental Biology*, *114*, 197–206.

Carter, B. R., Feely, R. A., Williams, N. L., Dickson, A. G., Fong, M. B., Takeshita, Y. (2018). Updated methods for global locally interpolated estimation of alkalinity, pH, and nitrate. *Limnology and Oceanography Methods*, *16*(2), 119–131.

Chavez, F., Pennington, J. T., Michisaki, R. P., Blum, M., Chavez, G. M., Friederich, J.,… Messié, M. (2017). Climate variability and change: Response of a coastal ocean ecosystem. *Oceanography*, *30*, 128–145.

Chen, P.-Y., Lin, A. Y.-M., McKittrick, J., Meyers, M. A. (2008). Structure and mechanical properties of crab exoskeletons. *Acta Biomaterialia*, *4*, 587–596.

Davis, S., Sylvia, G., Yochum, N., Cusack, C. (2017). Oregon Dungeness Crab Fishery Bioeconomic Model: A Fishery Interactive Simulator Learning Tool. Version 5.7. Prepared by Coastal Oregon Marine Experiment Station, Oregon State University and The Research Group, LLC for the Oregon Dungeness Crab Commission.

de la Haye, K. L., Spicer, J. I., Widdicombe, S., Briffa, M. (2011). Reduced sea water pH disrupts resource assessment and decision making in the hermit crab *Pagurus bernhardus*. *Animal Behaviour*, *82*, 495–501.

de la Haye, K. L., Spicer, J. I., Widdicombe, S., Briffa, M. (2012). Reduced pH sea water disrupts chemo-responsive behaviour in an intertidal crustacean. *Journal of Experimental Marine Biology and Ecology, 412*, 134–140.

Dissanayake, A., Ishimatsu, A. (2011). Synergistic effects of elevated CO_2 and temperature on the metabolic scope and activity in a shallow-water coastal decapod (*Metapenaeus joyneri*; Crustacea: Penaeidae). *ICES Journal of Marine Science, 68*, 1147–1154.

Dodd, J. R. (1964). Environmentally controlled variation in the shell structure of a pelecypod species. *Journal of Paleontology, 38*, 1065–1071.

Dodd, L. F., Grabowski, J. H., Piehler, M. F., Westfield, I., Ries, J. B. (2015). Ocean acidification impairs crab foraging behaviour. *Proceedings of the Royal Society B: Biological Sciences, 282*, 20150333.

Fabritius, H. O., Karsten, E. S., Balasundaram, K., Hild, S., Huemer, K., Raabe, D. (2012). Correlation of structure, composition and local mechanical properties in the dorsal carapace of the edible crab *Cancer pagurus*. *Zeitschrift für Kristallographie, 227*(11), 766–776.

Feely, R. A., Alin, S., Carter, B., Bednaršek, N., Hales, B., Chan, F., …, L. Juranek (2016). Chemical and biological impacts of ocean acidification along the west coast of North America. *Estuarine, Coastal and Shelf Science, 183*, 260–270.

Feely, R. A., Okazaki, R. R., Cai, W.-J., Bednaršek, N., Alin, S. R., Byrne, R. H., Fassbender, A. (2018). The combined effects of acidification and hypoxia on pH and aragonite saturation in the coastal waters of the California current ecosystem and the northern Gulf of Mexico. *Continental Shelf Research, 152*, 50–60.

633 Fernandes, J. A., Papathanasopoulou, E. , Hattam, C. , Queirós, A. M., Cheung, W. W., Yool, A.
634 , Artioli, Y. , Pope, E. C., Flynn, K. J., Merino, G. , Calosi, P. , Beaumont, N. , Austen, M.
635 C., Widdicombe, S., Barange, M. (2017). Estimating the ecological, economic and social
636 impacts of ocean acidification and warming on UK fisheries. *Fish and Fisheries*, *18*, 389–
637 411.

638 Fox, J., Weisberg, S. (2011). An R Companion to Applied Regression. USA: SAGE
639 Publications.

640 Giltz, S. M., Taylor, C.M. (2017). Reduced growth and survival in the larval Blue Crab
641 *Callinectes sapidus* under predicted ocean acidification. *Journal of Shellfish Research*, *36*,
642 481–485.

643 González-Gordillo, J. I., Rodríguez, A., Queiroga, H. (2004). Characterization of the megalopal
644 premoult stages of the Green crab, *Carcinus Maenas* (Decapoda, Portunidae), from
645 laboratory culture. *Journal of Crustacean Biology*, *24*, 502–510.

646 Gravinese, P. M., Enochs, I. C., Manzello, D. P., van Woesik, R. (2018). Warming and pCO_2
647 effects on Florida stone crab larvae. *Estuarine, Coastal and Shelf Science*, *204*, 193–201.

648 Gruber, N., Hauri, C., Lachkar, Z., Loher, D., Frölicher, T. L., Plattner, G.-K. (2012). Rapid
649 progression of ocean acidification in the California Current System. *Science*, *337*, 220–223.

650 Hans, S., Fehsenfeld, S., Treberg, J. R., Weihrauch, D. (2014). Acid–base regulation in the
651 Dungeness crab (*Metacarcinus magister*). *Marine Biology*, *161*, 1179–1193.

652 Henry, R. P., Kormanik, G. A., Smatresk, N. J., Cameron, J. N. (1981). The role of $CaCO_3$
653 dissolution as a source of HCO_3^- for the buffering of hypercapnic acidosis in aquatic and
654 terrestrial decapod crustaceans. *Journal of Experimental Biology*, *94*, 269–274.

Hobbs, R. C., Botsford, L. W., Thomas, A. (1992). Influence of hydrographic conditions and wind forcing on the distribution and abundance of Dungeness crab, *Cancer magister*, larvae. *Canadian Journal of Fisheries and Aquatic Sciences, 49*, 1379–1388.

Hodgson, E. E., Kaplan, I. C., Marshall, K. N., Leonard, J., Essington, T. E., Busch, D. S., Fulton, E. A., Harvey, C. J., Hermann, A. J., McElhany, P. (2018). Consequences of spatially variable ocean acidification in the California Current: Lower pH drives strongest declines in benthic species in southern regions while greatest economic impacts occur in northern regions. *Ecological Modelling, 383*, 106–117.

Jackson, T. M., O'Malley, K. G. (2017). Comparing genetic connectivity among Dungeness crab (*Cancer magister*) inhabiting Puget Sound and coastal Washington. *Marine Biology, 164*(6), 123.

Jackson, T. M., Roegner, G. C., O'Malley, K. G. (2018). Evidence for interannual variation in genetic structure of Dungeness crab (*Cancer magister*) along the California Current System. *Molecular Ecology*, *27*(2), 352–368.

Kaplan, I. C., Williams, G. D., Bond, N. A., Hermann, A. J., Siedlecki, S. A. (2016). Cloudy with a chance of sardines: Forecasting sardine distributions using regional climate models. *Fisheries Oceanography*, *25*, 15–27.

Kunkel, J. G., Nagel, W., Jercinovic, M. J. (2012). Mineral fine structure of the American lobster cuticle. *Journal of Shellfish Research, 31*, 515–526.

Lam, V. W. Y., Cheung, W. W. L., Reygondeau, G., Sumaila, U. R. (2016). Projected change in global fisheries revenues under climate change. *Scientific Reports, 6*, 32607.

Landes, A., Zimmer, M. (2012). Acidification and warming affect both a calcifying predator and prey, but not their interaction. *Marine Ecology Progress Series, 450*, 1–10.

Lindinger, M. I., Lauren, D. J., Mcdonald, D. G. (1984). Acid-base balance in the sea mussel, *Mytilus edulis*. III. Effects of environmental hypercapnia on intra- and extracellular acid-base balance. *Marine Biology Letters, 5*, 371–381.

Long, W. C., Swiney, K. M., Foy, R. J. (2016). Effects of high pCO_2 on Tanner crab reproduction and early life history, Part II: Carryover effects on larvae from oogenesis and embryogenesis are stronger than direct effects. *ICES Journal of Marine Science, 73*(3), 836–848.

Lowe, W. H., Allendorf, F. W. (2010). What can genetics tell us about population connectivity?. *Molecular Ecology*, *19*, 3038–3051.

Manno, C., Rumolo, P., Barra, M., d'Albero, S., Basilone, G., Genovese, S., Mazzola, S., Bonanno, A. (2019). Condition of pteropod shells near a volcanic CO_2 vent region. *Marine Environmental Research, 143*, 39–48.

Melzner, F., Gutowska, M. A., Langenbuch, M., Dupont, S., Lucassen, M., Thorndyke, M. C., Bleich, M., Pörtner, H. O. (2009). Physiological basis for high CO_2 tolerance in marine ectothermic animals: Pre-adaptation through lifestyle and ontogeny? *Biogeosciences, 6*(3), 4693–4738.

Michaelidis, B., Ouzounis, C., Paleras, A., Pörtner, H. (2005). Effects of long-term moderate hypercapnia on acid-base balance and growth rate in marine mussels *Mytilus galloprovincialis*. *Marine Ecology Progress Series, 293*, 109–118.

Miller, J. J., Maher, M., Bohaboy, E., Friedman, C. S., McElhany, P. (2016). Exposure to low pH reduces survival and delays development in early life stages of Dungeness crab (*Cancer magister*). *Marine Biology, 163*, 118.

Morgan, S. G. (1989). Adaptive significance of spination in estuarine crab Zoeae. *Ecology, 70*, 464–482. https://doi.org/10.2307/1937551

North, E. W., Schlag, Z., Hood, R. R., Li, M., Zhong, L., Gross, T., Kennedy, V. S. (2008). Vertical swimming behavior influences the dispersal of simulated oyster larvae in a coupled particle-tracking and hydrodynamic model of Chesapeake Bay. *Marine Ecology Progress Series, 359*, 99–115.

North, E. W., Adams, E. E., Schlag, Z., Sherwood, C. R., He, R., Hyun, K. H., Socolofsky, S. A. (2011). Simulating oil droplet dispersal from the *Deepwater Horizon* spill with a Lagrangian approach. In Y. Liu, A. Macfadyen, Z. Ji, & R. H. Weisberg (Eds.), Monitoring and Modeling the Deepwater Horizon Oil Spill: A Record Breaking Enterprise. *Geophysical Monograph Series* (pp. 217–226). USA: American Geophysical Union.

Oksanen, J., Blanchet, F. G., Friendly, M., Kindt, R., Legendre, P., McGlinn, D., … Wagner, H. (2019). Vegan: Community Ecology Package. R package version 2.5-5. Available at https://CRAN.R-project.org/package=vegan.

O'Malley, K. G., Corbett, K., Beacham, T. D., Jacobson, D. P., Jackson, T. M., Roegner, G. C. (2017). Genetic connectivity of the Dungeness crab (*Cancer magister*) across oceanographic regimes. *Journal of Shellfish Research, 36*(2), 453–465.

Pacific States Marine Fisheries Commission (2019). Species Report: Commercial Land Catch: Metric-Tons (mt), Revenue, and Price-per-pound (Price/lbs). Portland, OR: Pacific States

719 Marine Fisheries Commission. Available at
720 https://reports.psmfc.org/pacfin/f?p=501:1:5808950816361::NO::: Accessed 3/25/2019.

721 Paganini, A. W., Miller, N. A, Stillman, J. H. (2014). Temperature and acidification variability
722 reduce physiological performance in the intertidal zone porcelain crab *Petrolisthes cinctipes*.
723 *Journal of Experimental Biology, 217*(22), 3974–3980.

724 Page, T. M., Worthington, S., Calosi, P., Stillman, J. H. (2016). Effects of elevated pCO_2 on crab
725 survival and exoskeleton composition depend on shell function and species distribution: A
726 comparative analysis of carapace and claw mineralogy across four porcelain crab species
727 from different habitats. *ICES Journal of Marine Science, 74*(4), 1021–1032.

728 Pane, E., Barry, J. (2007). Extracellular acid-base regulation during short-term hypercapnia is
729 effective in a shallow-water crab, but ineffective in a deep-sea crab. *Marine Ecology*
730 *Progress Series, 334*, 1–9.

731 R Core Team (2019). R: A Language and Environment for Statistical Computing. R Foundation
732 for Statistical Computing. Available at https://www.R-project.org/.

733 Schiffer, M., Harms, L., Pörtner, H., Mark, F., Storch, D. (2014). Pre-hatching seawater pCO_2
734 affects development and survival of zoea stages of Arctic spider crab *Hyas araneus*. *Marine*
735 *Ecology Progress Series*, *501*, 127–139.

736 Schlag, Z. R., North, E. W. (2012). Lagrangian TRANSport model (LTRANS v.2) User's Guide.
737 Cambridge, Maryland: University of Maryland Center for Environmental Science, Horn
738 Point Laboratory.

739 Shanks, A. L. (1995). Mechanisms of cross-shelf dispersal of larval invertebrates and fish. In: L.
740 R. McEdward (Ed.), Ecology of Marine Invertebrate Larvae (pp. 324–367). USA: CRC
741 Press.

742 Siedlecki, S. A., Kaplan, I. C., Hermann, A. J., Nguyen, T. T., Bond, N. A., Newton, J. A.,
743 Williams, G. D., Peterson, W. T., Alin, S. R., Feely, R. A. (2016). Experiments with seasonal
744 forecasts of ocean conditions for the northern region of the California Current upwelling
745 system. *Scientific Reports, 6,* 27203.

746 Sinclair, M. (1988). Marine Populations: An Essay on Population Regulation and Speciation.
747 Washington Sea Grant. Seattle, Washington: University of Washington Press.

748 Small, D. P., Calosi, P., Boothroyd, D., Widdicombe, S., Spicer, J. I. (2015). Stage-specific
749 changes in physiological and life-history responses to elevated temperature and pCO_2 during
750 the larval development of the European lobster *Homarus gammarus* (L.). *Physiological and*
751 *Biochemical Zoology, 88,* 494–507.

752 Small, D. P., Calosi, P., Boothroyd, D., Widdicombe, S., Spicer, J. I. (2016). The sensitivity of
753 the early benthic juvenile stage of the European lobster *Homarus gammarus* (L.) to elevated
754 pCO_2 and temperature. *Marine Biology, 163,* 53.

755 Somero, G. N. (1986). Protons, osmolytes, and fitness of internal milieu for protein function.
756 *American Journal of Physiology–Regulatory, Integrative and Comparative Physiology, 251,*
757 R197–R213.

758 Somero, G. N., Beers, J. M., Chan, F., Hill, T. M., Klinger, T., Litvin, S. Y. (2015). What
759 changes in the carbonate system, oxygen, and temperature portend for the northeastern
760 Pacific Ocean: A physiological perspective. *BioScience, 66,* 14–26.

761 Spicer, J. I., Taylor, A. C. (1987). Carbon dioxide transport and acid-base regulation in the blood
762 of the beach-hopper *Orchestia gammarellus* (Pallas) (Crustacea: Amphipoda). *Ophelia, 28,*
763 49–61.

764 Spicer, J. I., Raffo, A. (2007). Widdicombe, S., Influence of CO_2-related seawater acidification
765 on extracellular acid–base balance in the velvet swimming crab *Necora puber*. *Marine*
766 *Biology, 151*, 1117–1125.

767 Sulkin, S. D. (1984). Behavioral basis of depth regulation in the larvae of brachyuran crabs.
768 *Marine Ecology Progress Series, 15,* 181–205.

769 Trigg, S. A., McElhany, P., Maher, M., Perez, D., Busch, D. S., Nichols, K. M. (1 August 2019).
770 Uncovering mechanisms of global ocean change effects on the Dungeness crab (*Cancer*
771 *magister*) through metabolomics analysis. *BioRxiv*, 574798.

772 Truchot, J. P. (1979). Mechanisms of the compensation of blood respiratory acid-base
773 disturbances in the shore crab, *Carcinus maenas* (L.). *Journal of Experimental Zoology, 210,*
774 407–416.

775 Tunnicliffe, V., Davies, K. T., Butterfield, D. A., Embley, R. W., Rose, J. M., Chadwick Jr, W.
776 W. (2009). Survival of mussels in extremely acidic waters on a submarine volcano. *Nature*
777 *Geoscience*, *2*, 344–348.

778 Turi, G., Lachkar, Z., Gruber, N., Münnich, M. (2016). Climatic modulation of recent trends in
779 ocean acidification in the California Current System. *Environmental Research Letters, 11,*
780 014007.

781 Walther, K., Anger, K., Pörtner, H. (2010). Effects of ocean acidification and warming on the
782 larval development of the spider crab *Hyas araneus* from different latitudes (54° vs. 79°N).
783 *Marine Ecology Progress Series, 417,* 159–170.

784 Wang, Y., Hu, M., Wu, F., Storch, D., Pörtner, H.-O. (2018). Elevated pCO_2 affects feeding
785 behavior and acute physiological response of the Brown Crab *Cancer pagurus*. *Frontiers in*
786 *Physiology, 9,*1164.

787

788

789

790

791

792

793

794

795

796

797

798

799

800

Figures

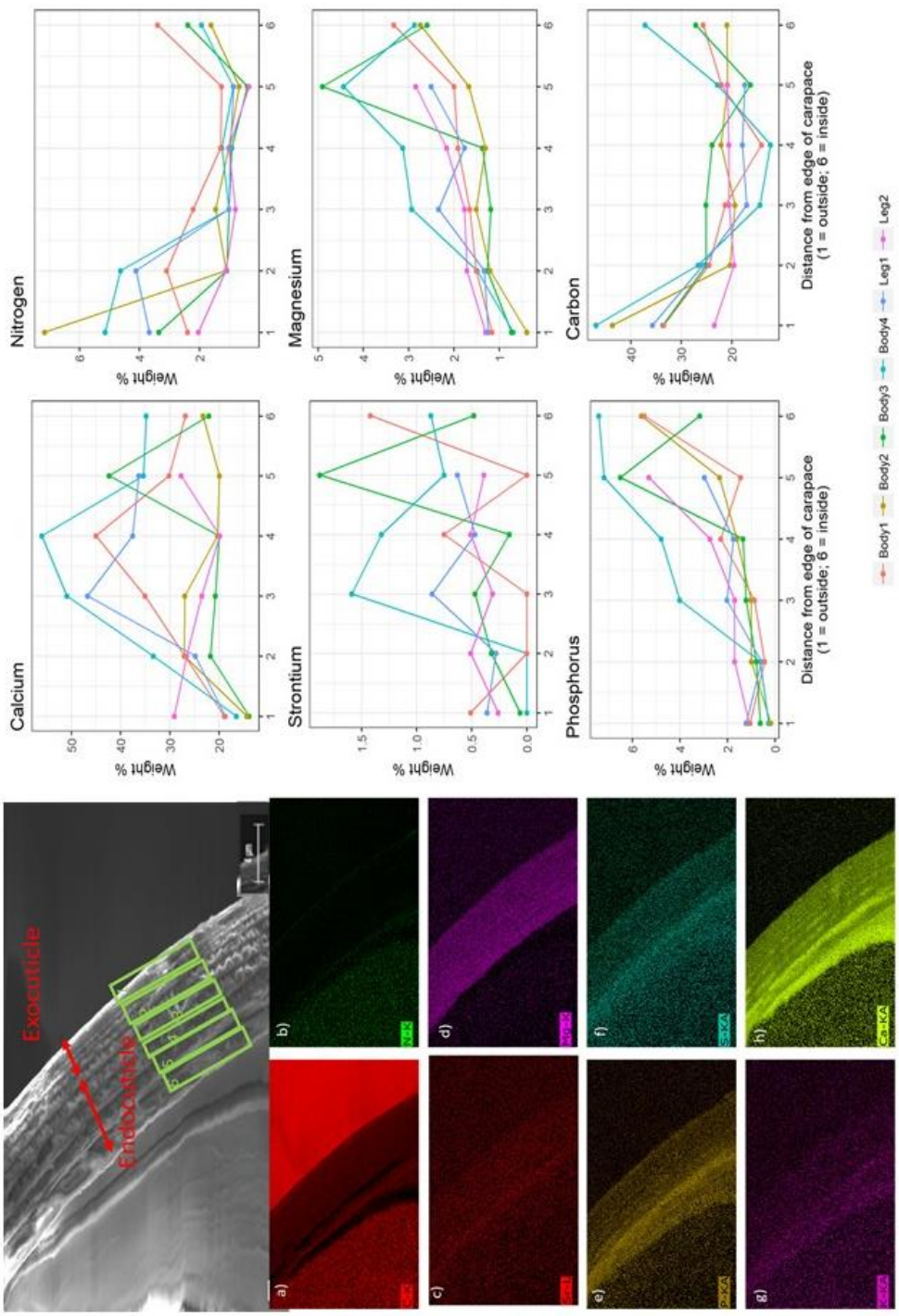

Figure 1: The cross sections of the Dungeness crab megalopae carapace and thickness (left panel; *a*) with increasing numbers describing the transition from the thinner exo- (1) to thinner endo-

cuticle (6). *b*) Distribution of various elements (C-carbon-a; N-nitrogen-b; Sr^{2+}- strontium-c; Mg^{2+}-magnesium-d; P-phosphor-e; S-sulphur-f; K-potassium-g, Ca^{2+}-calcium-h) from exo- (1) to endo-cuticle (6; right panel). The more intense colors depict higher elemental concentration. Spectrum and % content of selected elements in either carapace or pereopods (*c*). The numbers in (*a*) coincide with the numbers in *(b)* and (*c*) reflecting the position within the carapace.

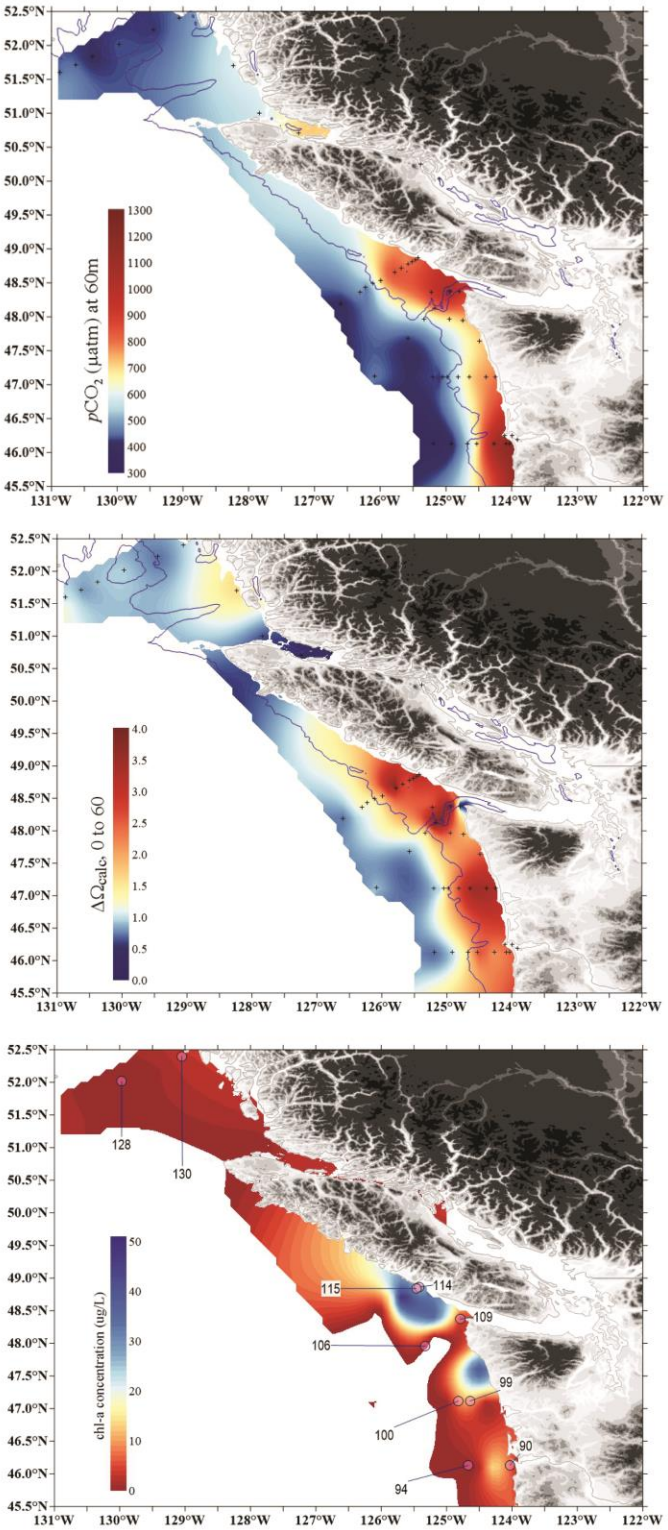

Figure 2: Interpolated $\Delta\Omega_{cal,60}$ (*a*) and $pCO_{2,60}$ (*b*) and chlorophyll (*c*) conditions in the onshore and offshore habitats along the US West Coast in June 2016. $\Delta\Omega_{cal,60}$ indicates the difference

between the surface and 60 m depth, while pCO_2 reflects the conditions at 60m depth. *c*) Chlorophyll distribution and concentration (chl-a; µg/L) demonstrate an order of magnitude difference between the regional nearshore and offshore region. The numbers indicate the stations at which the crabs were collected.

a)

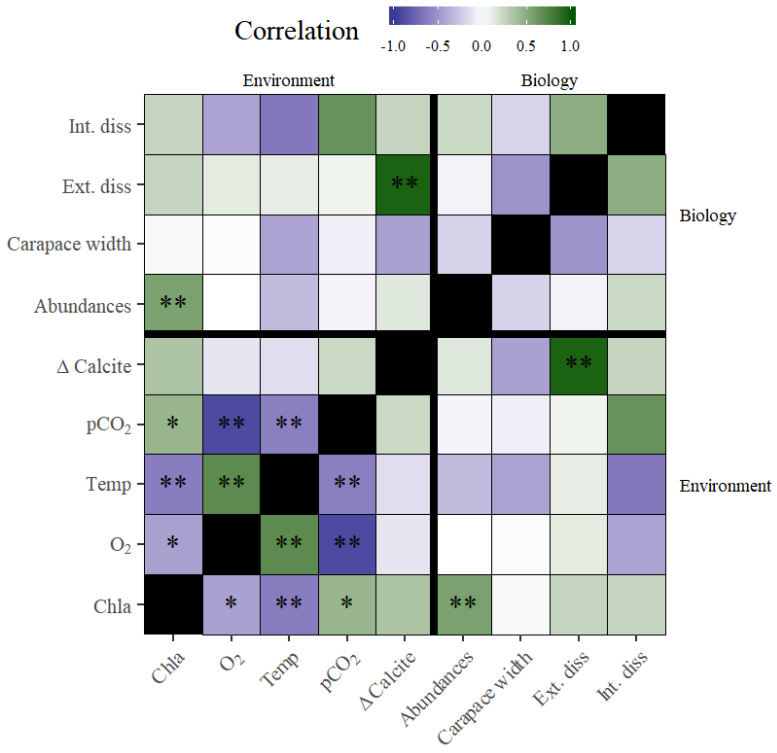

821

b)

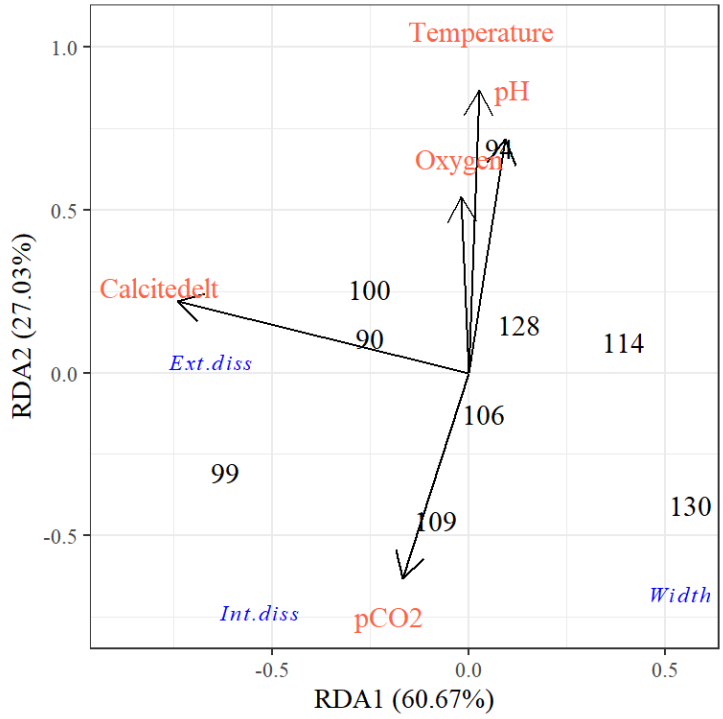

822

823 **Figure 3**: Correlation matrix of environmental variables and biological endpoints for Dungeness

824 megalopae: *(a)* Darker green values are strong positive correlations and darker purple values are

825 strong negative correlations, while dimmer green and purple indicate weaker correlations; and *b*)
826 Redundancy analyses (RDAs) for environmental variables used in the analyses with crab
827 biological measurements (internal and external dissolution, growth as carapace width).
828
829
830
831
832
833
834
835
836
837
838
839
840
841
842
843
844

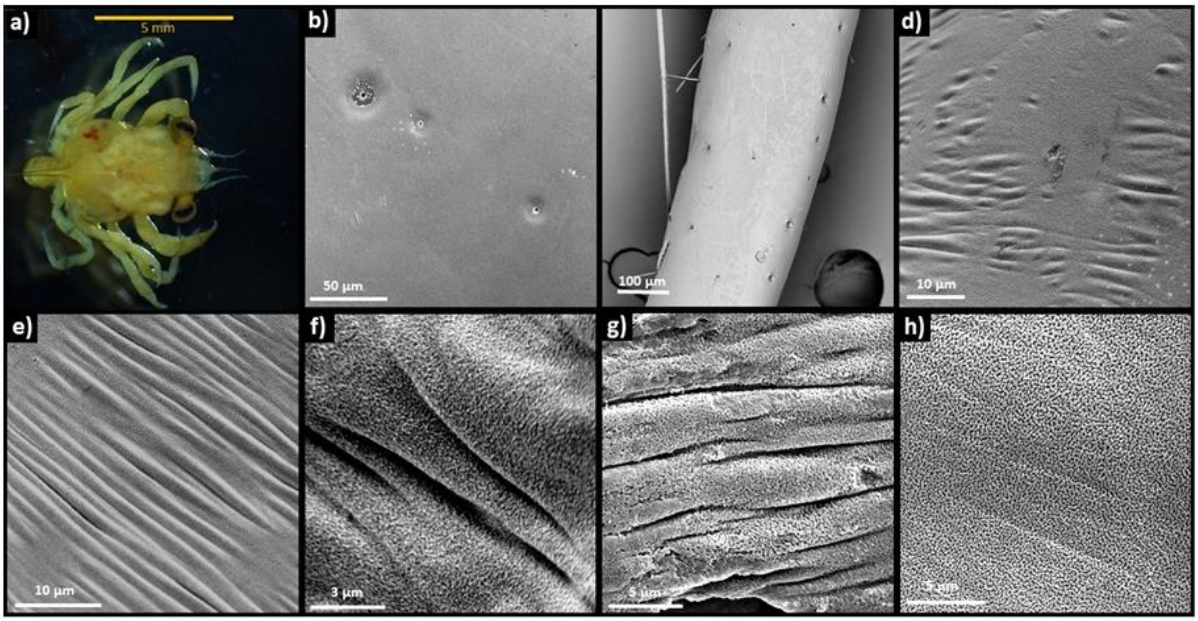

Figure 4: External carapace and pereopods of the Dungeness crab megalopae (*a*) in its undamaged form (*b*, *c*) and with dissolution presence ranging from mild (Stage 1; *d*) to severe (Stage 2; *e*, *f*) patterns on the carapace and pereopods showing similarity in the structural damages (*g*) or exposed crystals (*h*). Indicated is the scale of the measurements (µm).

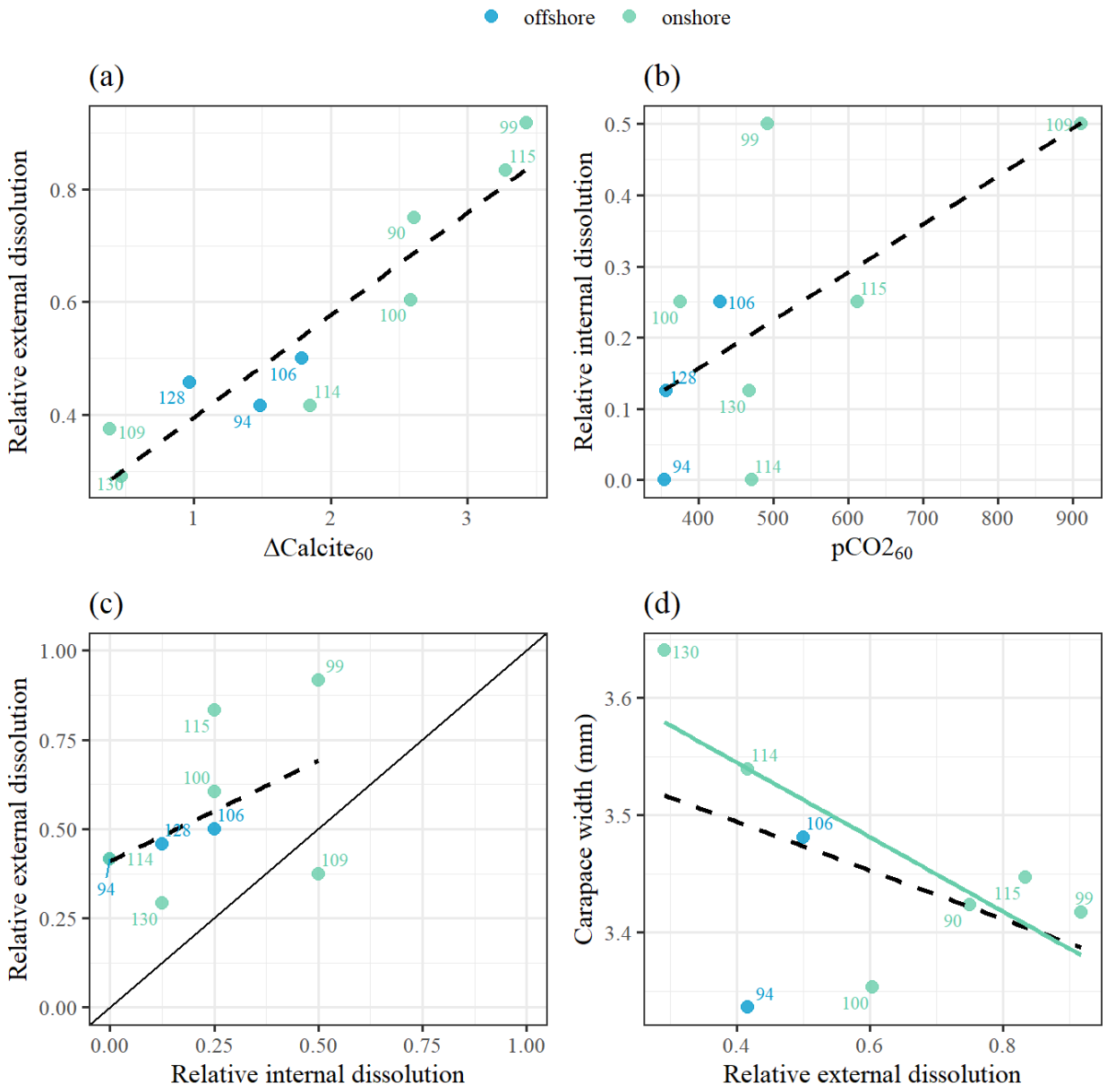

858

859

860 **Figure 5:** Estimated linear relationships between ocean-acidification gradients and dissolution.
861 Specifically for *a*) $\Delta\Omega_{cal,60}$ and relative external dissolution ($R^2 = 0.87$; $p < 0.001$); *b*) Depth-
862 integrated $pCO_{2,60}$ and relative internal dissolution ($R^2 = 0.41$; $p = 0.064$); *c*) Comparison of the
863 relative external and internal dissolution ($R^2 = 0.24$; $p = 0.18$); and *d*) Relative external
864 dissolution and carapace width ($R^2 = 0.57$; $p = 0.08$). Dotted lines show the linear regression fit

between all points. The solid line in (*c*) is the 1:1 line and the green line in (*d*) is the regression fit only through the onshore points. See methods for explanation of the term relative dissolution. Carapace width is in mm.

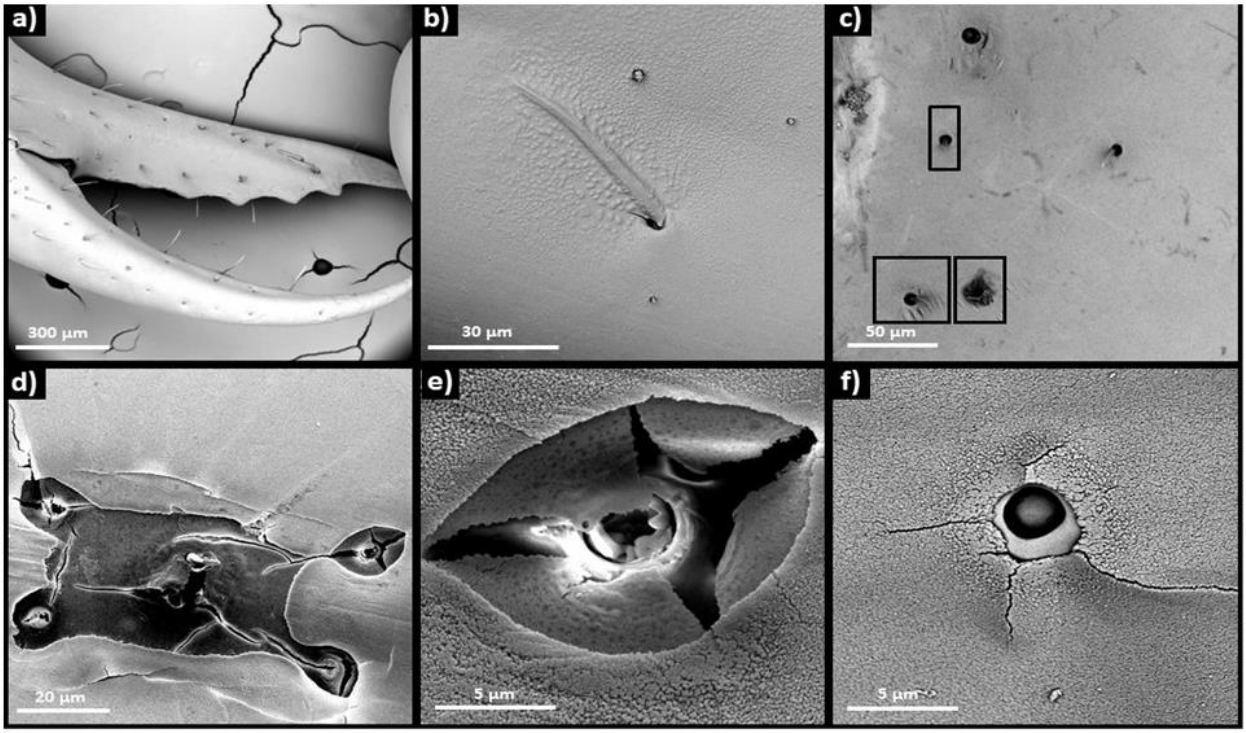

879

880

881 **Figure 6**: Presence of setae on the chelipeds (*a*) and carapace surface (*b*) of the megalopae on
882 the intact individuals. The exposure to greater $\Delta\Omega_{cal,60}$ differences mechanically damages the
883 setae and results in their absence and outrooting (black squares) because of the dissolution
884 around the neuritic canals (*d*, *f*) and damage with the collapsed structure (*e*).

885

886

887

888

889

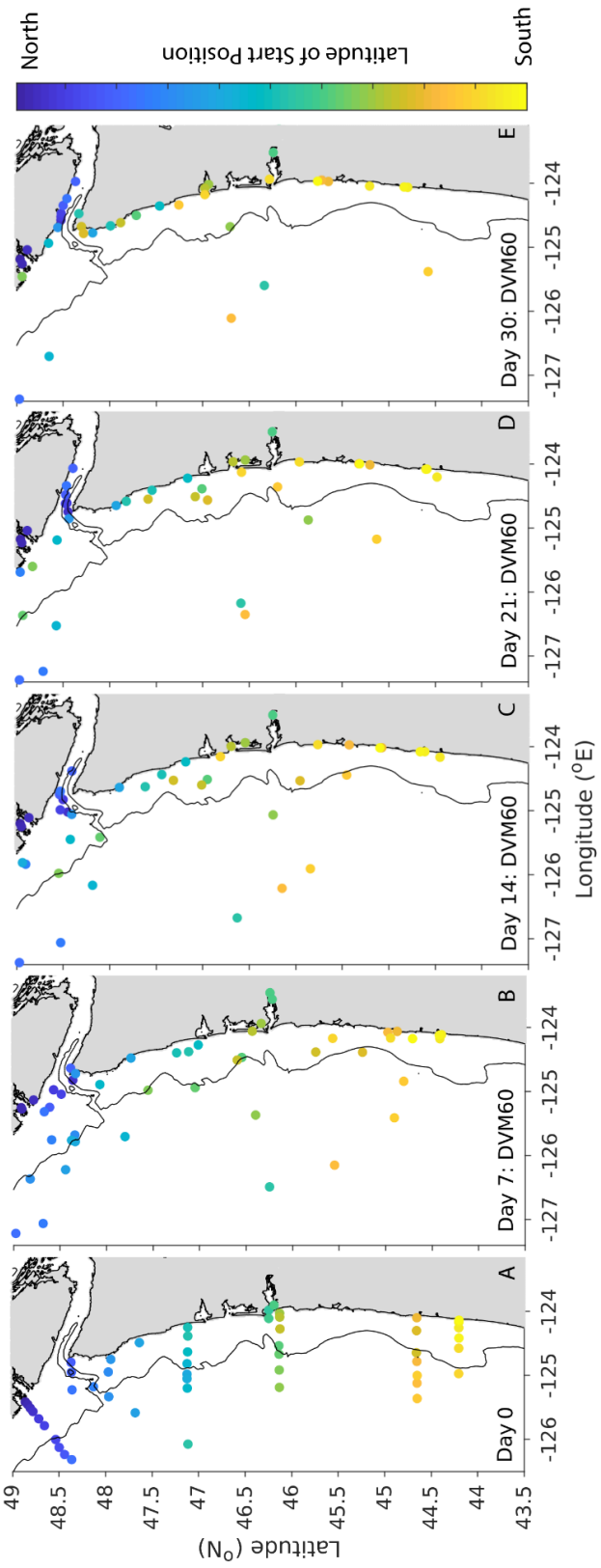

Figure 7: Particle initialization locations (*a*) and average backtracked locations (*b-e*) for 7, 14, 21, and 30-day simulated particles exhibiting diel vertical migration (DVM) between 0 and 60 m depths. Replicate particles (n=100) were initialized in the model at 51 locations representing the sampling stations for the 2016 West Coast Ocean Acidification Cruise. J-SCOPE's historical simulation of ocean conditions for 2016 was used to simulate advection of particles, and each particle exhibited vertical swimming between the ocean surface at night and a maximum daytime depth of 60 m. On a weekly basis, particle locations were averaged for all 100 particles initialized at the same station, which sometimes resulted in the average location being on land. These particles were moved to the nearest shoreline. Station color varies by transect for improved resolution of dispersal patterns occurring at different latitudes. The 200 m isobath is shown for reference, and land is shaded in grey.